ORIGINAL ARTICLE

Effects of (–)-MBP, a novel 5-HT$_{2C}$ agonist and 5-HT$_{2A/2B}$ antagonist/inverse agonist on brain activity: A phMRI study on awake mice

Preeti K. Sathe[1] | Gargi R. Ramdasi[1] | Kaylie Giammatteo[1] | Harvens Beauzile[1] | Shuyue Wang[1] | Heng Zhang[1] | Praveen Kulkarni[2] | Raymond G. Booth[1] | Craig F. Ferris[1,2,3]

[1]Department Pharmaceutical Sciences, Northeastern University, Boston, Massachusetts, USA

[2]Center for Translational Neuroscience, Northeastern University, Boston, Massachusetts, USA

[3]Department Psychology, Northeastern University, Boston, Massachusetts, USA

Correspondence
Craig F. Ferris, Center for Translational NeuroImaging, 360 Huntington Ave, Boston, MA 02115, USA.
Email: c.ferris@northeastern.edu

Abstract

A novel serotonin ligand (–)-MBP was developed for the treatment of schizophrenia that has 5-HT$_{2A/2B}$ antagonist activity together with 5-HT$_{2C}$ agonist activity. The multi-functional activity of this novel drug candidate was characterized using pharmacological magnetic resonance imaging. It was hypothesized (–)-MBP would affect activity in brain areas associated with sensory perception. Adult male mice were given one of three doses of (–)-MBP (3.0, 10, 18 mg/kg) or vehicle while fully awake during the MRI scanning session and imaged for 15 min post I.P. injection. BOLD functional imaging was used to follow changes in global brain activity. Data for each treatment were registered to a 3D MRI mouse brain atlas providing site-specific information on 132 different brain areas. There was a dose-dependent decrease in positive BOLD signal in numerous brain regions, especially thalamus, cerebrum, and limbic cortex. The 3.0 mg/kg dose had the greatest effect on positive BOLD while the 18 mg/kg dose was less effective. Conversely, the 18 mg/kg dose showed the greatest negative BOLD response while the 3.0 mg/kg showed the least. The prominent activation of the thalamus and cerebrum included the neural circuitry associated with Papez circuit of emotional experience. When compared to vehicle, the 3.0 mg dose affected all sensory modalities, for example, olfactory, somatosensory, motor, and auditory except for the visual cortex. These findings show that (–)-MBP, a ligand with both 5-HT$_{2A/2B}$ antagonist and 5-HT$_{2C}$ agonist activities, interacts with thalamocortical circuitry and impacts areas involved in sensory perception.

KEYWORDS
BOLD imaging, Papez circuit, schizophrenia, serotonin, thalamus

---

1 | INTRODUCTION

Serotonin (5-HT) is a neurotransmitter whose physiological effects are mediated by a family of 5-HT receptors (5-HTR). These receptors are categorized into seven classes (5-HT_1 to 5-HT_7) with each class being subdivided into further groups. The 5-HT_2 class is further divided into subtypes 5-HT_{2A}, 5-HT_{2B}, and 5-HT_{2C}. These 5-HT_2 (5-HT_{2R}) receptor subtypes are G protein-coupled receptors that act via Gαq/11 coupled activation of phospholipase C, leading to intracellular formation of inositol triphosphate and diacylglycerol and the release of calcium. 5-HT_{2A}R protein is highly expressed in the cortex and hippocampus and 5-HT_{2A}Rs have been targeted clinically to treat schizophrenia. 5-HT_{2B} receptors (5-HT_{2B}Rs) are largely found in smooth muscle tissue; however, they are also found in the cortex, hippocampus, cerebellum, lateral septum, hypothalamus, and medial amygdala of the brain, and they can modulate dopamine (as well as serotonin) neuronal function.[1–3] 5-HT_{2C} receptors (5-HT_{2C}Rs) are exclusively expressed in the central nervous system with high density in choroid plexus. 5-HT_{2C}Rs play a particularly important role in the ventral tegmentum, nucleus accumbens, and the prefrontal cortex[4] and have been targeted for treatment for various neuropsychiatric disorders such as schizophrenia, anxiety, depression, and addiction.[5]

First-generation antipsychotics, like haloperidol, are efficacious at treating psychosis but come with a host of serious off-target effects, including parkinsonism. Second-generation antipsychotics, often referred to as atypical antipsychotics, do not improve in efficacy and in fact have been shown to be ineffective in one-third of patients. An analysis of a new generation of drugs targeting the serotonin (5-HT) system, more specifically the 5-HT_{2C}R, as an alternative approach to treat psychoses could prove insightful.[6] Postmortem analysis of patients with a history of schizophrenia showed downregulation of 5-HT_{2C}Rs[7] and suggests a possible role in psychosis. 5-HT_{2A}Rs also may be involved in schizophrenia as blocking these receptors is one proposed mechanism of action of atypical antipsychotics.[8] Together, 5-HT_{2C}R agonism and 5-HT_{2A}R antagonism may provide a unique and efficacious mechanism for treating psychosis.

Booth and colleagues developed (–)-*trans*-(2*S*,4*R*)-4-(3′ [meta]-bromophenyl)-*N*,*N*-dimethyl-1,2,3,4-tetrahydronaphthalen-2-amine ((–)-MBP) which has agonist activity at 5-HT_{2C}Rs but competitive antagonist and inverse agonist activities at 5-HT_{2A}Rs and 5-HT_{2B}Rs,[6,9] To "fingerprint" or characterize the multi-functional serotonin 5-HT2R activities of this molecule, studies were performed on awake mice using blood oxygen level-dependent (BOLD) pharmacological magnetic resonance imaging (phMRI). This imaging protocol provides information on the integrated neural circuitry engaged by different doses of test compound when the mechanism of action is unknown due to multiple targets. For example, cannabidiol, CBD, is a promiscuous molecule whose mechanism is poorly understood due to its multiple targets.[10] In a recent study on awake mice, Sadaka et al. reported a dose-dependent effect of CBD that showed an unexpected polarization of brain activity between the hindbrain reticular activating system and the forebrain prefrontal cortex.[11] In this study using (–)-MBP, we found prominent dose-dependent changes in the thalamus, sensorimotor cortices, and limbic cortex. This confirmed our hypothesis that (–)-MBP would affect circuitry involved in sensory perception providing insight into possible therapeutic indications.

2 | MATERIALS AND METHODS

2.1 | Animal usage

Male C57BL/J6 mice ($n = 40$) approximately 100 days of age and weighing between 28 and 30 g were obtained from Charles River Laboratories. Mice were kept in a controlled environment where they experienced a 12-h cycle of light and darkness. The lights turned on at 07:00 h. They had unrestricted access to food and water. The mice were obtained and taken care of following the guidelines outlined in the "Guide for the Care and Use of Laboratory Animals" (National Institutes of Health Publications No. 85-23, Revised 1985). The study followed the regulations set by the Institutional Animal Care and Use Committee at Northeastern University, protocol # 21-0824R and complied with the ARRIVE guidelines, which provide recommendations for reporting in vivo experiments involving animal research.[12]

2.2 | Drug preparation and administration

(–)-MBP is a novel compound that functions as a near-full efficacy agonist at 5-HT_{2C} receptors and as an inverse agonist/antagonist at 5-HT_{2A} and 5-HT_{2B} receptor subtypes.[6,9] The compound was synthesized as previously described.[9,13] Affinities of (–)-MBP at mouse 5-HT_{2A} and 5-HT_{2C} receptors are Ki = 26 nM and Ki = 11 nM, respectively.[6] Affinity of (–)-MBP at the mouse 5-HT_{2B} receptor is not reported; however, Ki values for (–)-MBP at the human 5-HT_{2A}, 5-HT_{2B}, and 5-HT_{2C} receptors are 20, 13, and 12 nM, respectively.[3] (–)-MBP was dissolved in 0.9% NaCl for I.P. injections. Mice were randomly assigned to one of four groups corresponding to saline vehicle, 3.0, 10, or 18 mg/kg given in a volume of 100 μL. These doses were chosen based on the in vivo pharmacology reported by Canal et al. (2014) to block drug-induced head twitching and hyperlocomotion.[6] Lower doses of (–)-MBP, 0.1 and 1 mg/kg were ineffective. To deliver the drug remotely during the imaging session, a polyethylene tube (PE-20), approximately 30 cm in length, was positioned in the peritoneal cavity.

2.3 | Awake mouse imaging

A detailed description of the awake mouse imaging system is published elsewhere.[14] Notably, we used a quadrature transmit/receive volume coil (ID = 38 mm) that provided both high anatomical resolution and high signal-to-noise ratio for voxel-based BOLD fMRI. Furthermore, the unique design of the mouse holder (Ekam Imaging)

fully stabilized the head in a cushioned helmet, minimizing discomfort caused by ear bars and other restraint systems that are commonly used to immobilize the head for awake animal imaging.[15] A movie showing the set-up of a mouse for awake imaging is available at http://www.youtube.com/watch?v=W5Jup13isqw. The level of motion artifact combined for mice is shown in Figure 1. Mice with motion exceeding 100 μm, that is greater than one-half the in-plane dimensions of a voxel (ca 190 μm^2) in any orthogonal direction were excluded from the study. Based on these criteria and loss due to technical issues, the final number of mice in each experimental condition was vehicle ($n=6$), 3.0 mg/kg ($n=8$), 10 mg/kg ($n=7$), 18 mg/kg ($n=8$).

2.3.1 | Acclimation

One week before the initial imaging session, all the mice were familiarized with the head restraint and the noise produced by the scanner. Initially, the mice were gently secured in the holding system while under 1%–2% isoflurane anesthesia. Once they regained consciousness, the mice were placed in an enclosed black box designed to simulate an MRI scanner for a period of up to 30 min. This box emitted audio recordings of MRI pulses. This process of acclimation was repeated for four consecutive days in order to minimize the effects caused by the autonomic nervous system during awake animal imaging. The aim was to reduce changes in heart rate, respiration, corticosteroid levels, and motor movements, ultimately improving the quality of the images by enhancing the contrast-to-noise ratios.[16] Still other labs have focused on longer periods of acclimation to minimize stress during awake imaging.[15,17,18]

2.4 | BOLD phMRI image acquisition and pulse sequence

Experiments were conducted using a Bruker BioSpec 7.0T/20-cm USR horizontal magnet (Bruker) and a 2T/m magnetic field gradient insert (ID = 12 cm) capable of a 120-μsec rise time. At the beginning of each imaging session, a high-resolution anatomical data set was collected using the rapid acquisition relaxation enhancement (RARE) pulse sequence (RARE factor 8); (18 slices; 0.75 mm; field of view (FOV) 1.8 cm^2; data matrix 128 × 128; repetition time (TR) 2.1 s; echo time (TE) 12.4 msec; Effect TE 48 msec; number of excitations (NEX) 6; 6.5 min acquisition time). Functional images were acquired using a multi-slice Half Fourier Acquisition Single Shot Turbo Spin Echo (HASTE) pulse sequence (RARE factor 53); (18 slices; 0.75 mm; FOV 1.8 cm; data matrix 96 × 96; TR 6 s; TE 4 msec; Effective TE 24 msec; 20 min acquisition time; in-plane resolution 187.5 μm^2). To provide an illustration, the spatial resolution achieved is sufficient to distinguish the bilateral habenula region with approximately 4–5 voxels allocated for each side. However, it falls short in differentiating between the lateral and medial habenula. The utilization of spin echo was crucial in obtaining functional images that possessed the anatomical accuracy necessary for aligning the data with the mouse MRI atlas, as demonstrated in Figure 2. Each functional imaging session consisted of uninterrupted data acquisitions (whole brain scans) of 200 scan repetitions or acquisitions for a total elapsed time of 20 min. The control window included the first 50 scan acquisitions (18 slices acquired in each), covering a 5 min baseline. Following the control window, an I.P. injection of vehicle or (−)-MBP was given followed by another 150 acquisitions over a 15 min period. The order of drug doses was randomized over the scanning sessions and blind to the imager which was also true during data analysis.

2.5 | Imaging data analysis

The dose-dependent effect of (−)-MBP on brain activity was quantified through positive and negative percent changes in BOLD signal relative to baseline. The initial analyses of signal change in individual subjects were done comparing image acquisitions 100–200 to baseline 1–50. The statistical significance of these alterations was evaluated for each voxel (approximately 15 000 per subject) in their original reference system using independent Student's t-tests.
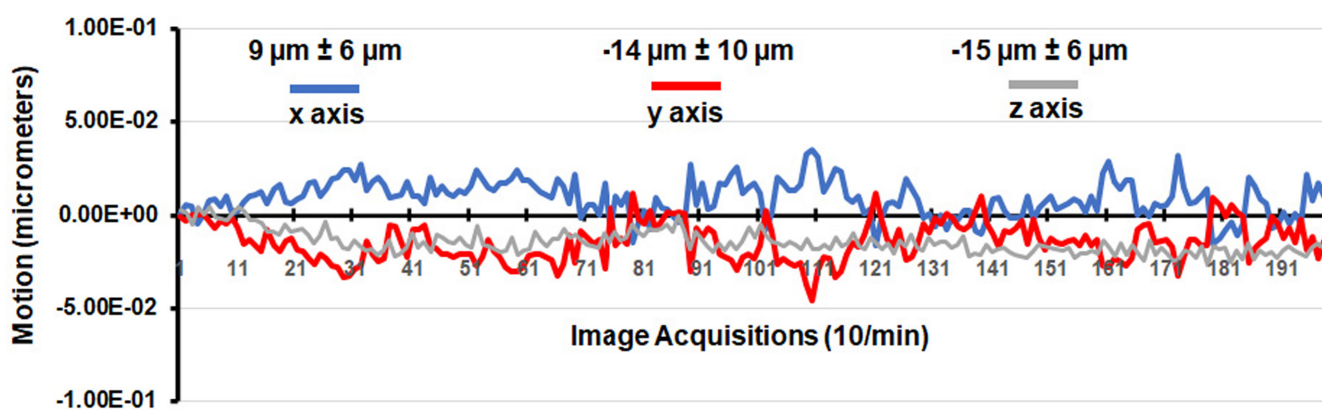

FIGURE 1 Motion artifact. Shown is the degree of motion artifact recorded over the 20 min imaging protocol (200 image acquisitions). The data are reported as the mean and standard deviation in micrometers for axes Y, Z, and X for all mice from each experimental condition ($n=29$).
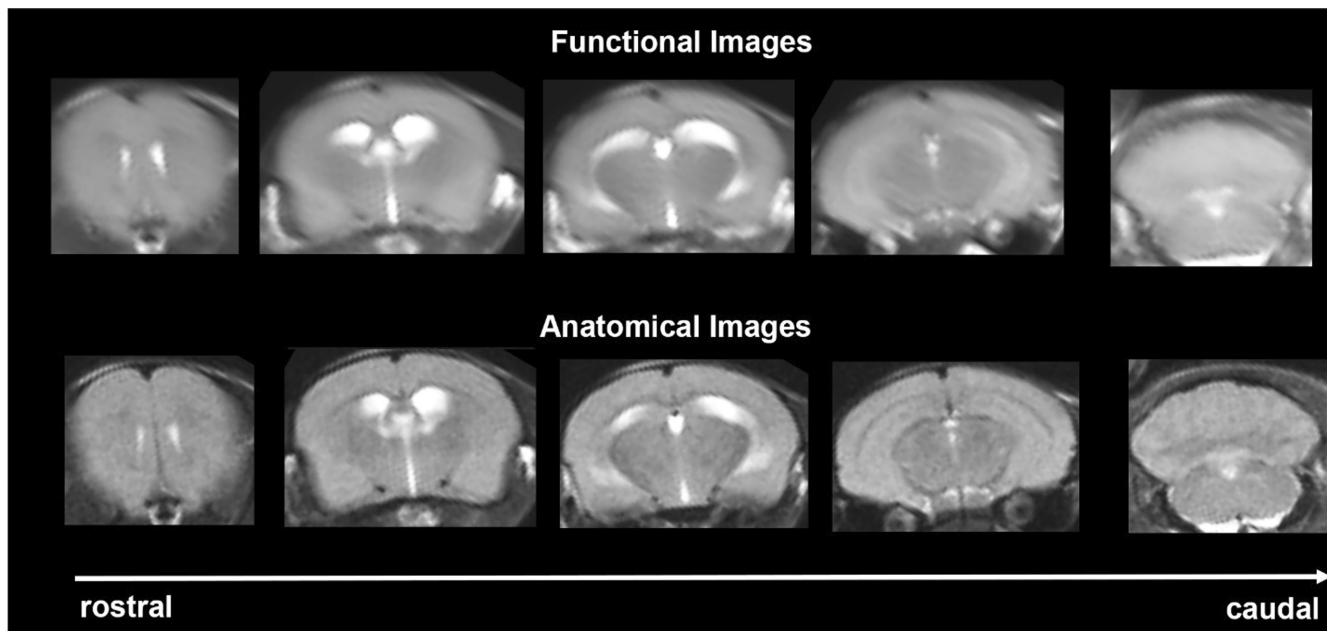
FIGURE 2 Neuroanatomical fidelity. Shown are representative examples of brain images collected during a single imaging session using a multi-slice spin echo, RARE (rapid acquisition with relaxation enhancement) pulse sequence. The row on the bottom shows axial sections collected during the anatomical scan taken at the beginning of each imaging session using a data matrix of 18 slices; 0.75 mm thickness; FOV 1.8 cm^2; data matrix 128×128. The row above shows the same images but collected for functional analysis using HASTE, a RARE pulse sequence modified for faster acquisition time. These images were acquired using the same field of view and slice anatomy but a larger data matrix of 96×96. Note the anatomical fidelity between the functional images and their original anatomical image. The absence of any distortion is necessary when registering the data to atlas to resolve 132 segmented brain areas.

A threshold of 1% was employed to accommodate the typical fluctuations in the BOLD signal observed in the awake rodent brain. To address the issue of multiple t-tests conducted, a mechanism was implemented to control false-positive detections, as described by Genovese et al.[19] This mechanism aimed to maintain the average false-positive detection rate below 0.05. The formula used for this purpose was as follows:

$$P_i \le \frac{i}{V} \frac{q}{c(V)}, \tag{1}$$

In our analysis, the formula used to control false positives involved evaluating the p-values (P_i) obtained from the t-tests for each pixel within the region of interest (ROI). The ROI contained a total of V pixels, and these pixels were ranked based on their probability values. To maintain conservative estimates of significance, a false-positive filter value (q) of 0.2 was applied. Additionally, the constant c(V) was set to unity, following the approach outlined by Benjamini and Hochberg.[20] The resulting statistical significance was determined based on a 95% confidence level, two-tailed distributions, and the assumption of heteroscedastic variance for the t-tests. Pixels that displayed statistical significance retained their relative percentage change values, while all other pixel values were assigned a value of zero.

Voxel-based percent changes in BOLD signal generated for individual subjects were combined across subjects within the same group to build representative functional maps. To this end, all images were first aligned and registered to a 3D Mouse Brain Atlas© with 132 segmented and annotated brain regions (Ekam Solutions). The co-registrational code SPM8 was used with the following parameters: Quality: 0.97, Smoothing: 0.35 mm, Separation: 0.50 mm. Gaussian smoothing was performed with a FWHM of 0.8 mm. Image registration involved translation, rotation, and scaling, independently and in all three dimensions. All applied spatial transformations were compiled into a matrix $[T_j]$ for the j-th subject. Every transformed anatomical pixel location was tagged with a brain area to generate fully segmented representations of individual subjects within the atlas.

Next, composite maps of the percent changes in BOLD signal were built for each experimental group. Each composite pixel location (row, column, and slice) was mapped to a voxel of the j-th subject by virtue of the inverse transformation matrix $[T_j]^{-1}$. A tri-linear interpolation of subject-specific voxel values determined their contribution to the composite representation. The use of the inverse matrices ensured that the full composite volume was populated with subject inputs. The average of all contributions was assigned as the percent change in BOLD signal at each voxel within the composite representation of the brain for the respective experimental group. The number of activated voxels in each of the 132 regions was then compared between the control and (−)-MBP doses using a Kruskal-Wallis test statistic. Those brain areas with significant changes in positive and negative BOLD signal are presented in Tables 1 and 2. The data for all 132 brain areas for both positive and negative BOLD are presented in Files S1 and S2. The data from the Files S1 and S2

TABLE 1 (−)-MBP positive volume of activation dose response.

Positive BOLD volume of activation								
Brain area	3 mg	SE	10 mg	SE	18 mg	SE	p value	ω Sq
Lateral posterior thalamus	35	1.4	26	2.5	18	3.3	.001	0.730
Posterior thalamus	39	0.8	28	3.9	23	4.0	.001	0.686
Secondary somatosensory ctx	214	3.1	166	18.3	138	22.7	.001	0.620
Reticular thalamus	40	0.8	32	2.4	27	4.2	.001	0.607
Corpus callosum	167	3.8	129	13.3	94	14.9	.001	0.606
Anterior cingulate area	123	2.3	88	12.5	75	12.4	.001	0.585
Insular caudal ctx	94	4.4	58	8.1	53	5.4	.001	0.575
Olfactory tubercles	64	1.9	53	5.3	42	4.4	.002	0.533
Globus pallidus	102	2.4	87	5.5	66	11.0	.002	0.528
Internal capsule	61	1.5	50	5.0	35	5.3	.002	0.503
Zona incerta	35	1.7	27	1.5	20	3.3	.002	0.494
Medial geniculate	51	2.5	45	2.2	34	3.6	.002	0.492
External capsule	51	1.9	42	3.9	30	4.4	.002	0.489
Anterior thalamus	57	1.5	52	1.5	38	6.4	.004	0.450
Primary somatosensory ctx	782	17.9	683	59.7	585	77.4	.004	0.446
Pontine reticular n. caudal	162	10.6	127	11.7	97	13.7	.005	0.415
Lateral geniculate	29	1.0	23	2.9	18	2.1	.005	0.042
Principal sensory n. trigeminal	99	6.0	82	5.9	50	12.1	.007	0.391
Primary motor ctx	197	11.4	166	21.4	146	21.5	.007	0.382
Ventral thalamus	206	2.5	183	10.2	152	24.3	.008	0.372
Auditory ctx	142	5.2	126	7.2	114	9.9	.008	0.369
Lateral caudal hypothalamus	45	2.4	32	4.3	38	1.3	.008	0.056
Caudate putamen	684	13.5	599	66.0	505	77.5	.009	0.362
Rostral piriform ctx	272	12.5	230	28.5	162	19.8	.009	0.358
Retrosplenial rostral ctx	154	4.0	126	12.5	106	17.8	.009	0.358
Insular rostral ctx	196	10.8	162	25.2	116	19.6	.011	0.339
Lateral dorsal thalamus	34	2.8	29	2.8	19	3.4	.011	0.337
Ventral pallidum	80	2.2	60	6.6	62	4.8	.013	0.326
Granular cell layer	192	28.0	162	25.5	100	15.7	.013	0.322
Superior colliculus	314	8.4	297	17.1	214	35.6	.014	0.321
Ventral tegmental area	24	1.1	16	3.3	18	0.9	.015	0.057
6th cerebellar lobule	217	12.3	156	15.9	125	25.6	.015	0.309
Pontine reticular n. oral	144	6.8	116	9.9	110	13.8	.018	0.294
Bed n. stria terminalis	59	0.8	46	4.3	43	7.5	.018	0.063
Glomerular layer	237	35.8	196	31.3	109	17.7	.019	0.289
Diagonal band of Broca	25	0.7	22	2.3	19	1.0	.020	0.284
Central medial thalamus	21	1.3	16	1.6	14	3.0	.021	0.280
Paraventricular hypothalamus	6	0.5	4	0.5	3	0.8	.021	0.039
Anterior olfactory area	238	34.8	201	30.8	165	23.9	.023	0.269
Dorsal hippocampal commissure	10	0.6	9	0.8	6	1.1	.023	2.000
Lateral preoptic area	13	0.6	9	0.6	11	2.0	.029	0.342
Parietal ctx	13	0.9	8	1.3	9	1.8	.038	0.078
Orbital ctx	191	28.4	184	26.0	153	23.1	.041	0.213

(Continues)

TABLE 1 (Continued)

Positive BOLD volume of activation							
Brain area	3 mg	SE	10 mg	SE	18 mg	SE	p value	ω Sq
Endopiriform area	29	3.3	23	3.6	17	3.2	.041	0.213
Subiculum	253	18.6	212	10.1	201	20.3	.041	0.015
Mesencephalic reticular formation	262	11.8	234	7.8	202	24.0	.050	0.194

TABLE 2 (−)-MBP negative volume of activation dose response.

Negative BOLD volume of activation							
Brain area	3 mg	SE	10 mg	SE	18 mg	SE	p value	ω Sq
Anterior thalamus	0	0.0	0	0.2	8	2.8	.001	0.559
Insular rostral ctx	0	0.3	10	5.7	41	7.7	.001	0.543
Primary motor ctx	0	0.0	0	0.4	4	1.3	.001	0.502
Medial geniculate	0	0.0	2	1.5	5	1.7	.002	0.485
Secondary somatosensory ctx	0	0.0	4	2.9	16	5.2	.003	0.480
Olfactory tubercles	0	0.1	1	1.3	8	2.3	.003	0.451
Corpus callosum	0	0.4	9	3.9	32	6.5	.003	0.469
Primary somatosensory ctx	1	0.5	7	4.4	41	10.4	.003	0.444
Retrosplenial rostral ctx	0	0.0	6	3.7	15	4.8	.004	0.404
Endopiriform area	0	0.0	0	0.1	3	1.9	.005	0.345
Medial dorsal thalamus	0	0.0	0	0.0	2	0.7	.005	0.277
Anterior cingulate area	0	0.0	3	2.1	4	1.4	.006	0.411
Internal capsule	0	0.3	2	1.0	8	3.5	.008	0.372
Rostral piriform ctx	4	4.4	10	6.5	46	11.4	.012	0.323
External capsule	0	0.3	2	1.5	6	1.5	.014	0.326
Frontal association ctx	0	0.3	7	4.9	10	3.3	.018	0.237
Zona incerta	0	0.0	2	1.2	4	1.7	.018	0.290
Central medial thalamus	0	0.0	0	0.0	1	0.4	.024	0.141
Posterior thalamus	0	0.0	0	0.0	1	0.9	.024	0.250
Reticular thalamus	0	0.0	1	0.6	4	2.5	.026	0.257
Pontine reticular n. caudal	2	1.4	1	0.7	8	3.3	.027	0.263
Principal sensory n. trigeminal	2	1.1	4	2.1	19	6.4	.027	0.257
Solitary tract area	2	1.4	1	0.6	11	6.0	.031	0.197
CA1	1	0.9	23	9.6	33	9.2	.031	0.206
Insular caudal ctx	0	0.3	7	3.4	15	4.7	.031	0.263
Ventral thalamus	0	0.0	2	2.4	10	7.7	.032	0.195
CA3	2	1.6	6	2.9	17	6.8	.036	0.196
Caudate putamen	4	2.6	16	10.5	53	22.4	.037	0.225
Granular cell layer	0	0.0	16	12.6	5	2.0	.038	0.206
Inferior colliculus	1	0.5	4	2.5	18	7.5	.038	0.180
3rd cerebellar lobule	0	0.3	2	1.2	7	2.9	.039	0.178
Secondary motor ctx	0	0.0	1	0.4	2	0.7	.039	0.162
Olivary complex	0	0.3	0	0.0	2	1.1	.039	0.146
10th cerebellar lobule	0	0.2	1	0.4	6	3.3	.040	0.193
Auditory ctx	0	0.0	3	1.2	6	2.5	.042	0.203
Dentate gyrus	1	0.8	4	2.0	9	3.2	.044	0.166
Accumbens shell	0	0.0	1	1.0	3	1.5	.049	0.119

on all 132 individual brain areas were then coalesced into brain regions, for example cerebellum, thalamus, hypothalamus, basal ganglia, etc. For example, the thalamus shown in Figure 3 is comprised of 11 brain areas as listed in Table 3. The number of voxels activated for each brain across the four doses was normalized and presented as a percentage of the total volume of all voxels as shown in Figure 3. Each measure for the four experimental groups was compared with a one-way ANOVA followed by Tukey's multiple comparison test using GraphPad Prism version 9.1.2 for Windows, (GraphPad Software).

3 | RESULTS

Tables reporting the positive and negative volumes of activation, that is number of voxels activated for all 132 brain areas for vehicle and each dose of (−)-MBP are provided in Files S1 and S2. There was a robust positive activation with drug as 102/132 brain areas were significantly different across the four experimental groups. When the three doses of (−)-MBP were compared to each other, a clear dose-dependent change in positive volume of activation was observed in 46/132 brain areas as shown in Table 1. The brain areas in
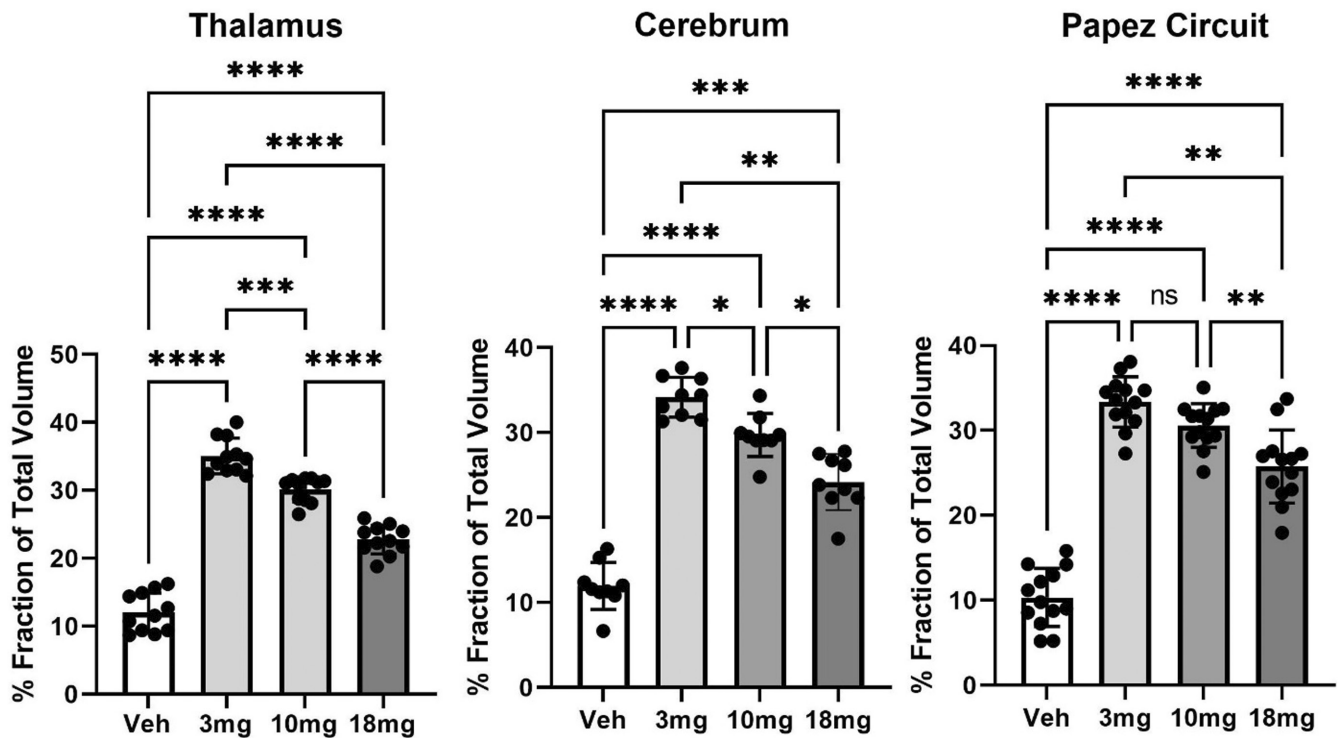

FIGURE 3 Dose-dependent effects of (−)-MBP. Shown are bar graphs (mean ± SD) and dot plots (brain areas) presented as the mean of percent fraction of the total volume of activation in each brain area across all experimental conditions. The inverse response to each dose of (−)-MBP is significantly different from vehicle and each other with the exception of the 3.0 and 10 mg doses in Papez circuit. *<.05; **<.01; ***<.001; ****<.0001.

TABLE 3 Dose-dependent changes in thalamus.

Positive BOLD volume of activation								
Brain area	3 mg	SE	10 mg	SE	18 mg	SE	p value	ω Sq
Lateral posterior thalamus	35	1.4	26	2.5	18	3.3	.001	0.730
Posterior thalamus	39	0.8	28	3.9	23	4.0	.001	0.686
Reticular thalamus	40	0.8	32	2.4	27	4.2	.001	0.607
Zona incerta	35	1.7	27	1.5	20	3.3	.002	0.494
Medial geniculate	51	2.5	45	2.2	34	3.6	.002	0.492
Anterior thalamus	57	1.5	52	1.5	38	6.4	.004	0.450
Lateral geniculate	29	1.0	23	2.9	18	2.1	.005	0.042
Ventral thalamus	206	2.5	183	10.2	152	24.3	.008	0.372
Lateral dorsal thalamus	34	2.8	29	2.8	19	3.4	.011	0.337
Central medial thalamus	21	1.3	16	1.6	14	3.0	.021	0.280

Table 1 are ranked in order of their significance. Shown highlighted in gray are the mean number of voxels significantly activated following the I.P. injection of vehicle (Veh), 3, 10, and 18 mg/kg of (−)-MBP with a critical value $\alpha < .05$ and the omega square (ω Sq) for effect size. A false discovery rate (FDR) for multi-comparisons gives a significance level of $p = .069$. Note the trend in activation across all brain areas with the 3 mg/kg dose being the most active and the 18 mg/kg dose the least active. Shown in Table 2 highlighted in gray are the dose-dependent changes in negative volume of activation. Only 29/132 brain areas showed a significant difference across doses (FDR = 0.044). Interestingly, there was little to no negative BOLD signal change with the 3 and 10 mg/kg doses of (−)-MBP, while the highest dose of 18 mg/kg caused the greatest increase in negative BOLD. The trends would suggest that the positive and negative volume of activation are inversely correlated with the 18 mg/kg dose showing the lowest positive activation but the highest negative response. It should be noted that mice administered the 3 mg/kg dose of (−)-MBP were observed to be devoid of movement and non-reactive to toe pinch for approximately 15–20 min after being removed from the magnet or approximately 30 min after drug administration. This behavior was not observed with the 10 and 18 mg/kg doses.

The brain areas most represented in Table 1 are localized to the thalamus and cerebral cortex. Tables 2 and 3 list these areas, while Figure 3 shows bar graphs (mean ± SD) and dot plots (brain areas) for each dose of (−)-MBP and vehicle for thalamus and cerebral cortex. A one-way ANOVA showed a significant ($p < .0001$) difference between doses for thalamus ($F_{(2.183,21.83)} = 144.3$) and cerebral cortex ($F_{(2.520,20.16)} = 82.11$). Tukey's multiple comparisons showed all doses for each brain region were significantly different from vehicle and from each other (Table 4).

Figure 4a shows the rat equivalent of Papez circuit and its different brain areas as color-coded 3D volumes. These areas are coalesced as a single volume in yellow below with the average positive BOLD signal shown in red for vehicle and the 3.0 mg dose of (−)-MBP. Figure 4b is 2D activation maps showing the average

positive BOLD signal change as individual voxels displayed on the mouse MRI segmented atlas. The BOLD signal change for vehicle and 3.0 mg/kg (−)-MBP for each voxel is the average of all areas shown in the table (Figure 4c) that comprise Papez circuit. The table lists all these areas in order of their significance (critical value <0.05) and effect size (omega square). The anterior thalamus (highlighted in gray) is considered the key node in Papez circuit. The time course in BOLD signal change in the anterior thalamus for vehicle and each dose of (−)-MBP is shown in Figure 4d. I.P injections occurred at approximately the 50th image acquisition (5 min from onset of imaging). A repeated measures mixed effects analysis showed a main effect for treatment ($F_{(3,24)} = 6.424$, $p < .0024$) and a significant interaction between time and treatment ($F_{(597,4776)} = 3.810$, $p < .0001$).

4 | DISCUSSION

The present study evaluated the dose-dependent changes in BOLD signal across the entire mouse brain in response to a serotonin ligand (−)-MBP that is a near-full efficacy agonist at 5-HT$_{2C}$ receptors and an inverse agonist/antagonist at 5-HT$_{2A}$ and 5-HT$_{2B}$ receptor subtypes. BOLD imaging in awake rodents has been used to characterize the immediate effects of numerous drugs on brain activity.[11,15,21,22] In this case, the fingerprint or pattern of BOLD activity across 132 brain areas represents a complex interaction between different serotonin receptors across discrete brain areas. Pharmacological MRI is a method to assess the global integrated neural circuitry underpinning the behavioral effects of CNS therapeutics independent of their specific biochemical mechanism.[23] In this study, 74/132 brain areas showed a dose-dependent change in activation predominantly in thalamus, cerebrum, and limbic circuitry. These data are discussed with respect to serotonergic signaling in neural circuitry that may be involved in psychiatric illness, particularly psychosis.

5HT$_{2C}$ receptors have a widespread distribution in the brain, whereas 5HT$_{2A}$ receptors are concentrated in a few areas such

TABLE 4 Dose-dependent changes in cerebral cortex.

Positive BOLD volume of activation								
Brain area	3 mg	SE	10 mg	SE	18 mg	SE	*p* value	ω Sq
Secondary somatosensory ctx	214	3.1	166	18.3	138	22.7	.001	0.620
Anterior cingulate ctx	123	2.3	88	12.5	75	12.4	.001	0.585
Insular caudal ctx	94	4.4	58	8.1	53	5.4	.001	0.575
Primary somatosensory ctx	782	17.9	683	59.7	585	77.4	.004	0.446
Primary motor ctx	197	11.4	166	21.4	146	21.5	.007	0.382
Auditory ctx	142	5.2	126	7.2	114	9.9	.008	0.369
Rostral piriform ctx	272	12.5	230	28.5	162	19.8	.009	0.358
Retrosplenial rostral ctx	154	4.0	126	12.5	106	17.8	.009	0.358
Insular rostral ctx	196	10.8	162	25.2	116	19.6	.011	0.339
Parietal ctx	13	0.9	8	1.3	9	1.8	.038	0.078
Orbital ctx	191	28.4	184	26.0	153	23.1	.041	0.213

(a)

Limbic Cortex
"Papez Circuit of Emotional Experience"

(c)

Positive BOLD Volume of Activation					
Brain Area	Veh	3.0 mg	10 mg	18 mg	P val	Ω Sq
anterior cingulate ctx	29	120	96	77	0.001	0.553
anterior thalamus	14	57	52	41	0.001	0.506
primary somatosensory ctx	326	786	742	671	0.001	0.501
insular caudal ctx	34	91	60	54	0.002	0.481
entorhinal ctx	144	572	482	449	0.003	0.432
rostral piriform ctx	116	287	265	146	0.004	0.406
secondary motor ctx	71	204	185	175	0.005	0.394
retrosplenial caudal ctx	47	153	152	128	0.007	0.361
medial mammillary n.	4	21	27	25	0.007	0.359
insular rostral ctx	72	204	191	124	0.009	0.337
prelimbic ctx	9	51	54	58	0.009	0.331
orbital ctx	46	211	206	171	0.010	0.329
caudal piriform ctx	81	172	141	118	0.055	0.179

(b)

Papez Circuit

(d)

FIGURE 4 Circuit of Papez. (a) Shows the color-coded 3D volumes that comprise Papez circuit. These volumes are coalesced into a single yellow volume below showing the average positive BOLD signal (red) from all subjects. (b) To the right is 2D activation maps from the rat brain atlas showing the precise location of the significantly positive (red) BOLD voxels. Each voxel is the average signal from all subjects for vehicle or 3.0 mg dose of (−)-MBP. The table in (c) is the brain areas that comprise Papez circuit ranked in order of significance. The time course plot in (d) to the right shows the percent change in BOD signal for the anterior thalamus for each experimental condition over the 20 min scanning session. Arrow denotes time of I.P. injection. Vertical lines denote SE.

as the cortex, and both receptors show overlapping distribution in some areas.[24] Multiple reports have mentioned the presence of both $5HT_{2A}$ and $5HT_{2C}$ receptors in thalamic regions such as lateral and medial geniculate nucleus, reticular nucleus, and zona incerta.[24-26] Given the presence of both receptors in thalamus, the observed decreasing dose response may be attributed to inactivation of $5HT_{2A}$ receptors at low concentration (due to $5\text{-}HT_{2A}$ antagonism/inverse agonism) and activation of $5HT_{2C}$ receptors (due to $5\text{-}HT_{2C}$ agonism) at high concentration. An expected outcome of a $5HT_{2C}$ agonist alone would have been a dose-dependent

increase in activation in regions with high $5HT_{2C}$ receptor expression. However, multiple factors might be responsible for the decreasing negative BOLD signal, dose response observed in this study, as (−)-MBP also has a competitive antagonist effect at the histamine H_1 receptor.[6] The present study showed activation of nearly all of the cerebrum. It is reported that there is significant colocalization of both receptors in rat medial prefrontal cortex with a higher concentration of $5HT_{2A}$.[27]

In this study, (−)-MBP activated nearly all areas of the thalamus. There was a significant decreasing BOLD signal, dose–response

with the exception of the anterior pretectal nucleus and parafascicular nucleus. Previous studies have shown that $5\text{-}HT_{2C}Rs$ are widely distributed and abundant in the thalamus of rodents including the parafascicular nucleus.[28] This inconsistency may be due to the presence of $5\text{-}HT_{2A}Rs$ in the parafascicular nucleus, whose deactivation by (–)-MBP is masking the excitation of $5\text{-}HT_{2C}Rs$ in this region.[29] Our current results align well with what is known about the distribution of $5\text{-}HT_{2A}$ and $5\text{-}HT_{2C}$ receptors in the thalamus. The thalamus acts as a filter for sensory input before relaying this information to the cortex.[30] $5\text{-}HT_{2A}Rs$ and $5\text{-}HT_{2C}Rs$ have both proven to be prominent targets for mood-related disorders.[31] Given the known role of the thalamus as a sensory filter, (–)-MBP's activation of the thalamus should increase its ability to filter sensory input prior to relaying it to the cortex. Together, the known information about $5\text{-}HT_{2A}Rs$, $5\text{-}HT_{2C}Rs$, as well as the thalamus' function, suggests that (–)-MBP may be efficacious in diseases and disorders where the thalamus's activity is downregulated, or sensory input is upregulated.

The activation of the anterior nucleus of the thalamus together with other midline dorsal thalamic nuclei (e.g., paraventricular, medial dorsal, and central nuclei) is particularly interesting because the anterior nucleus is the cornerstone of the neural circuitry of emotion first proposed by Cannon[32] and popularized by Papez.[33] The "Papez circuit" connects the hypothalamus and hippocampus to the limbic cortex through the anterior thalamus and midline dorsal thalamic nuclei. These thalamic nuclei receive extensive afferent connections from the hippocampus[34,35] and the mammillary nuclei.[36] These midline thalamic nuclei send primary projections to the anterior cingulate, retrosplenial, prefrontal, and orbital cortices and adjacent cortical areas. The rodent equivalent of the Papez circuit was described by Kulkarni et al., while imaging the innate response to the highly attractive smell of almond in rats.[37] Indeed, we have used the almond-induced pattern of BOLD activation described by Kulkarni et al., to create the circuit of Papez shown in Figure 4.

As noted above, mice administered the 3.0 mg/kg dose of (–)-MBP were observed to be devoid of movement and non-reactive to toe pinch for approximately 15–20 min after being removed from the magnet, or approximately 30 min after drug administration. This observation is difficult to explain given the published findings that (–)-MBP lacks sedative and locomotor effects.[6] This outcome may be related to $5\text{-}HT_{2C}$ receptor negative modulation of dopamine release.[38] It has been reported that $5HT_{2C}R$ agonism mediates tonic inhibition of frontal-cortical dopaminergic transmission.[39] A previous study has shown that selective $5\text{-}HT_{2C}R$ antagonists have the potential to reverse haloperidol-induced catalepsy with a significant increase of $5HT_{2C}R$ levels in medial dorsal thalamus.[38] Reavill et al. found that $5HT_{2C}Rs$ play an important role in catalepsy.[40] Given the activation of the medial dorsal thalamus by (–)-MBP in this current study, and (–)-MBP's known action as a $5\text{-}HT_{2C}R$ agonist, we speculate that dopamine levels were decreased by the agonistic activity of (–)-MBP at $5\text{-}HT_{2C}Rs$, thus inhibiting motion and pain response of the mice.

This is consistent with the results of previous behavioral studies in which selective $5HT_{2C}R$ agonists cause a decrease in locomotor activity in mice, while $5\text{-}HT_{2A}$ agonists cause an increase in locomotor activity.[41] Likewise, the $5\text{-}HT_{2B}$ inverse agonist/antagonist activity of (–)-MBP should be considered regarding its effects on locomotor activity. For example, 5-HT antagonists reduce PCP-induced hyperlocomotion (without inducing catalepsy) and reduce amphetamine-induced hyperlocomotion in rats.[3,42] Another possible mechanism for the decrease in locomotion at low doses of (–)-MBP might be the involvement of histamine H_1 receptors, a potential off-target where (–)-MBP has appreciable affinity, $Ki = 30 nM$.[13] The absence of locomotor effects at higher doses of (–)-MBP used in the current studies is puzzling, but nonetheless bodes well for beneficial psychotropic effects without locomotor and sedative effects.

4.1 | Data interpretation

Ideally, brain and blood should have been collected at the end of the imaging session to ascertain the actual levels of (–)-MBP at each dose. The choice of drug doses in phMRI is usually based on preclinical behavioral pharmacology. In this case, the dose range was taken from Canal et al., looking at the ability of (–)-MBP to block the head twitching effect of 5HT2 agonists and amphetamine-induced hyperlocomotion in male C57BL/J6 mice.[6] The 10 mg/kg dose of (–)-MBP was effective in significantly decreasing both behavioral measures by 10 min after administration. The present study shows a dose-dependent decrease in positive BOLD in thalamus and cortex within 15 min of drug administration that could explain the blocking effects of (–)-MBP. Canal et al. reported doses of 0.1 and 1.0 mg/kg of (–)-MBP were ineffective in blocking drug-induced head twitching and hyperlocomotion. It would have been interesting to see if these lower doses would have caused a dose-dependent increase in positive BOLD creating an inverted U-shaped dose-response curve.

5 | SUMMARY

The present study was performed using phMRI in mice treated with (–)-MBP and showed a dose-dependent decrease in BOLD signal in brain regions, especially thalamus, cerebrum, and limbic cortex. With respect to serotonergic signaling the pattern of neural activation based on previous literature would suggest (–)-MBP might have therapeutic efficacy in psychiatric illness, particularly psychosis. $5\text{-}HT_{2A}R$ antagonism has been associated with antipsychotic-like effects.[43] Indeed, clozapine, a highly effective atypical antipsychotic, acts through antagonism of $5\text{-}HT_{2A}Rs$ and multiple dopamine receptors, with many off-target effects including histamine H_1 receptors and $5\text{-}HT_{2C}Rs$. Given the agonism of (–)-MBP at $5\text{-}HT_{2C}Rs$, antagonism at $5\text{-}HT_{2A}Rs$, and its robust thalamic/cortical response that entails Papez circuit, this drug may have benefits similar to clozapine but with fewer side effects. Also, further attention should be

paid to the cortical feedback to the thalamic reticular nucleus that exerts GABAergic control over the primary thalamic projections to sensory and motor cortices aiding in filtering and regulating sensory neurotransmission.

AUTHORS' CONTRIBUTIONS

This work was done by graduate students Preeti K. Sathe, Gargi R. Ramdasi, Kaylie Giammatteo, Harvens Beauzile, Shuyue Wang, and Heng Zhang, to satisfy a course requirement. All contributed equally to the data generation, analysis, and manuscript preparation. Praveen Kulkarni, Raymond G. Booth, and Craig F. Ferris contributed to the concept, experimental design, drafting, manuscript preparation, and interpretation.

CONFLICT OF INTEREST STATEMENT

Craig F. Ferris has a financial interest in Animal Imaging Research, a company that makes radiofrequency electronics and holders for awake animal imaging. Craig F. Ferris and Praveen Kulkarni have a partnership interest in Ekam Solutions a company that develops 3D MRI atlases for animal research.

DATA AVAILABILITY STATEMENT

The original contributions presented in this study are included in the article/Supplementary material, further inquiries can be directed to the corresponding author.

ETHICS STATEMENT

The protocol (# 21-0824R) used in this study complied with the regulations of the Institutional Animal Care and Use Committee at Northeastern University.

ORCID

Craig F. Ferris https://orcid.org/0000-0001-9744-5214

REFERENCES

1. Cathala A, Lucas G, Lopez-Terrones E, Revest JM, Artigas F, Spampinato U. Differential expression of serotonin(2B) receptors in GABAergic and serotoninergic neurons of the rat and mouse dorsal raphe nucleus. *Mol Cell Neurosci*. 2022;121:103750. doi:10.1016/j.mcn.2022.103750
2. Devroye C, Cathala A, Piazza PV, Spampinato U. The central serotonin(2B) receptor as a new pharmacological target for the treatment of dopamine-related neuropsychiatric disorders: rationale and current status of research. *Pharmacol Ther*. 2018;181:143-155. doi:10.1016/j.pharmthera.2017.07.014
3. Devroye C, Cathala A, Haddjeri N, et al. Differential control of dopamine ascending pathways by serotonin2B receptor antagonists: new opportunities for the treatment of schizophrenia. *Neuropharmacology*. 2016;109:59-68. doi:10.1016/j.neuropharm.2016.05.024
4. Wold EA, Wild CT, Cunningham KA, Zhou J. Targeting the 5-HT2C receptor in biological context and the current state of 5-HT2C receptor ligand development. *Curr Top Med Chem*. 2019;19:1381-1398. doi:10.2174/1568026619666190709101449
5. Hoyer D, Hannon JP, Martin GR. Molecular, pharmacological and functional diversity of 5-HT receptors. *Pharmacol Biochem Behav*. 2002;71:533-554. doi:10.1016/s0091-3057(01)00746-8
6. Canal CE, Morgan D, Felsing D, et al. A novel aminotetralin-type serotonin (5-HT) 2C receptor-specific agonist and 5-HT2A competitive antagonist/5-HT2B inverse agonist with preclinical efficacy for psychoses. *J Pharmacol Exp Ther*. 2014;349:310-318. doi:10.1124/jpet.113.212373.PMC3989798
7. Chagraoui A, Thibaut F, Skiba M, Thuillez C, Bourin M. 5-HT2C receptors in psychiatric disorders: a review. *Progr Neuro-Psychopharmacol Biol Psychiatry*. 2016;66:120-135. doi:10.1016/j.pnpbp.2015.12.006
8. Felsing DE, Anastasio NC, Miszkiel JM, Gilbertson SR, Allen JA, Cunningham KA. Biophysical validation of serotonin 5-HT2A and 5-HT2C receptor interaction. *PLoS One*. 2018;13:e0203137. doi:10.1371/journal.pone.0203137
9. Casey AB, Mukherjee M, McGlynn RP, Cui M, Kohut SJ, Booth RG. A new class of 5-HT(2A) /5-HT(2C) receptor inverse agonists: synthesis, molecular modeling, in vitro and in vivo pharmacology of novel 2-aminotetralins. *Br J Pharmacol*. 2022;179:2610-2630. doi:10.1111/bph.15756
10. McPartland JM, Duncan M, Di Marzo V, Pertwee RG. Are cannabidiol and Delta(9)-tetrahydrocannabivarin negative modulators of the endocannabinoid system? A systematic review. *Br J Pharmacol*. 2015;172:737-753. doi:10.1111/bph.12944.PMC4301686
11. Sadaka AH, Ozuna AG, Ortiz RJ, et al. Cannabidiol has a unique effect on global brain activity: a pharmacological, functional MRI study in awake mice. *J Transl Med*. 2021;19:220. doi:10.1186/s12967-021-02891-6.PMC8142641
12. Kilkenny C, Browne W, Cuthill IC, Emerson M, Altman DG; Group NCRRGW. Animal research: reporting in vivo experiments: the ARRIVE guidelines. *Br J Pharmacol*. 2010;160:1577-1579. doi:10.1111/j.1476-5381.2010.00872.x.PMC2936830
13. Sakhuja R, Kondabolu K, Cordova-Sintjago T, et al. Novel 4-substitute d-N,N-dimethyltetrahydronaphthalen-2-amines: synthesis, affinity, and in silico docking studies at serotonin 5-HT2-type and histamine H1 G protein-coupled receptors. *Bioorg Med Chem*. 2015;23:1588-1600. doi:10.1016/j.bmc.2015.01.060.PMC4363177
14. Ferris CF, Kulkarni P, Toddes S, Yee J, Kenkel W, Nedelman M. Studies on the Q175 Knock-in model of Huntington's disease using functional imaging in awake mice: evidence of olfactory dysfunction. *Front Neurol*. 2014;5:94. doi:10.3389/fneur.2014.00094.PMC4074991
15. Ferris CF. Applications in awake animal magnetic resonance imaging. *Front Neurosci*. 2022;16:854377. doi:10.3389/fnins.2022.854377.PMC9017993
16. King JA, Garelick TS, Brevard ME, et al. Procedure for minimizing stress for fMRI studies in conscious rats. *J Neurosci Methods*. 2005;148:154-160. doi:10.1016/j.jneumeth.2005.04.011.PMC2962951
17. Stenroos P, Paasonen J, Salo RA, et al. Awake rat brain functional magnetic resonance imaging using standard radio frequency coils and a 3D printed restraint kit. *Front Neurosci*. 2018;12:548. doi:10.3389/fnins.2018.00548.PMC6109636
18. Chang PC, Procissi D, Bao Q, Centeno MV, Baria A, Apkarian AV. Novel method for functional brain imaging in awake minimally restrained rats. *J Neurophysiol*. 2016;116:61-80. doi:10.1152/jn.01078.2015.PMC4961750
19. Genovese CR, Lazar NA, Nichols T. Thresholding of statistical maps in functional neuroimaging using the false discovery rate. *Neuroimage*. 2002;15:870-878. doi:10.1006/nimg.2001.1037

20. Benjamini Y, Hochberg Y. Controlling the false discovery rate: a practical and powerful approach to multiple testing. *J R Stat Soc B Methodol*. 1995;57:289-300.

21. Ferris CF, Kulkarni P, Yee JR, Nedelman M, de Jong IEM. The serotonin receptor 6 antagonist Idalopirdine and acetylcholinesterase inhibitor donepezil have synergistic effects on brain activity-a functional MRI study in the awake rat. *Front Pharmacol*. 2017;8:279. doi:10.3389/fphar.2017.00279.PMC5467007

22. Ferris CF, Yee JR, Kenkel WM, et al. Distinct BOLD activation profiles following central and peripheral oxytocin administration in awake rats. *Front Behav Neurosci*. 2015;9:245. doi:10.3389/fnbeh.2015.00245.PMC4585275

23. Borsook D, Becerra L, Hargreaves R. A role for fMRI in optimizing CNS drug development. *Nat Rev Drug Discov*. 2006;5:411-424. doi:10.1038/nrd2027

24. Pompeiano M, Palacios JM, Mengod G. Distribution of the serotonin 5-HT2 receptor family mRNAs: comparison between 5-HT2A and 5-HT2C receptors. *Mol Brain Res*. 1994;23:163-178.

25. Hoffman BJ, Mezey E. Distribution of serotonin 5-HT1C receptor mRNA in adult rat brain. *FEBS Lett*. 1989;247:453-462. doi:10.1016/0014-5793(89)81390-0

26. Nichols DE. Psychedelics. *Pharmacol Rev*. 2016;68:264-355. doi:10.1124/pr.115.011478.PMC4813425

27. Nocjar C, Alex KD, Sonneborn A, Abbas AI, Roth BL, Pehek EA. Serotonin-2C and -2a receptor co-expression on cells in the rat medial prefrontal cortex. *Neuroscience*. 2015;297:22-37.

28. Clemett DA, Punhani T, S. Duxon M, Blackburn TP, Fone KCF. Immunohistochemical localisation of the 5-HT2C receptor protein in the rat CNS. *Neuropharmacology*. 2000;39:123-132. doi:10.1016/s0028-3908(99)00086-6

29. Chung KKMM, Herbert J. Central serotonin depletion modulates the behavioural, endocrine and physiological responses to repeated social stress and subsequent c-fos expression in the brains of male rats. *Neuroscience*. 1999;92:613-625.

30. Yasuno F, Suhara T, Okubo Y, et al. Low dopamine D2Receptor binding in subregions of the thalamus in schizophrenia. *Am J Psychiatry*. 2004;161:1016-1022. doi:10.1176/appi.ajp.161.6.1016

31. Julius D, Huang KN, Livelli TJ, Axel R, Jessell TM. The 5HT2 receptor defines a family of structurally distinct but functionally conserved serotonin receptors. *Proc Natl Acad Sci*. 1990;87:928-932. doi:10.1073/pnas.87.3.928

32. Cannon WB. The James-Lang theory of emotion: a critical examination and an alternative theory. *Am J Psychol*. 1927;39:106-124.

33. Papez JW. A proposed mechanism of emotion. *Arch Neurol Psychiatry*. 1937;38:725-743.

34. Sikes RW, Chronister RB, White LE. Origin of the direct hippocampus-anterior thalamic bundle in the rat: a combined horseradish peroxidase-Golgi analysis. *Exp Neurol*. 1977;57:379-395.

35. Swanson LW, Cowan WM. An autoradiographic study of the organization of the efferent connections of the hippocampal formation in the rat. *J Comp Neurol*. 1977;172:49-84.

36. Seki M, Zyo K. Anterior thalamic afferents from the mamillary body and the limbic cortex in the rat. *J Comp Neurol*. 1984;229:242-256.

37. Kulkarni P, Stolberg T, Sullivanjr JM, Ferris CF. Imaging evolutionarily conserved neural networks: preferential activation of the olfactory system by food-related odor. *Behav Brain Res*. 2012;230:201-207. doi:10.1016/j.bbr.2012.02.002

38. Creed-Carson M, Oraha A, Nobrega JN. Effects of 5-HT2A and 5-HT2C receptor antagonists on acute and chronic dyskinetic effects induced by haloperidol in rats. *Behav Brain Res*. 2011;219:273-279. doi:10.1016/j.bbr.2011.01.025

39. Millan M, Dekeyne A, Gobert A. Serotonin (5-HT) 2C receptors tonically inhibit dopamine (DA) and noradrenaline (NA), but not 5-HT, release in the frontal cortex in vivo. *Neuropharmacology*. 1998;37:953-955.

40. Reavill C, Kettle A, Holland V, Riley G, Blackburn TP. Attenuation of haloperidol-induced catalepsy by a 5-HT2Creceptor antagonist. *Br J Pharmacol*. 1999;126:572-574. doi:10.1038/sj.bjp.0702350

41. Halberstadt AL, Van Der Heijden I, Ruderman MA, et al. 5-HT2A and 5-HT2C receptors exert opposing effects on locomotor activity in mice. *Neuropsychopharmacology*. 2009;34:1958-1967. doi:10.1038/npp.2009.29

42. Auclair AL, Cathala A, Sarrazin F, et al. The central serotonin 2B receptor: a new pharmacological target to modulate the mesoaccumbens dopaminergic pathway activity. *J Neurochem*. 2010;114:1323-1332. doi:10.1111/j.1471-4159.2010.06848.x

43. Lally J, Gaughran F, Timms P, Curran SR. Treatment-resistant schizophrenia: current insights on the pharmacogenomics of antipsychotics. *Pharmgenomics Pers Med*. 2016;9:117-129. doi:10.2147/PGPM.S115741.PMC5106233

SUPPORTING INFORMATION

Additional supporting information can be found online in the Supporting Information section at the end of this article.